Chapter 4

ab initio simulations of amorphous carbon nitrides

Density functional *ab initio* molecular dynamics is used to study the incorporation of nitrogen into amorphous carbon networks. The networks were analysed using the maximally-localised Wannier function technique for producing a localised orbital picture which provides a means of identifying bonding types of the nitrogen and carbon atoms within the disordered structures. Addition of nitrogen was found to cause a decrease in the fraction of sp^3-bonded carbon and this effect was most severe at high density. These changes to carbon bonding are not confined to the immediate vicinity of a nitrogen atom. The structure, elastic and electronic properties of the networks are examined and compared with existing simulations and experimental observations. It was found that removing electrons from the networks caused structural changes which could explain the two-state conductivity in amorphous carbon nitride memory devices.

4.1 Introduction

In previous chapters the structure and electronic properties of amorphous carbon nitrides were studied, revealing that nitrogen was bonding into a predominantly sp^2

bonded carbon network. A simple structural model was proposed to explain the experimental results. Research by other laboratories showed it was possible to deposit $a-$C:N with high sp^3-carbon fractions with no decrease in this fraction as nitrogen was added. This prompted questions of :

- Experimental studies discussed in Chapter 3 suggested nitrogen could be evolving from the amorphous matrix - did nitrogen form dimers at low density ?
- How was nitrogen incorporated - did it form an sp^2 network with surrounding carbon atoms, or was it incorporated as an sp^2 or sp^3 with a lone-pair.
- Did nitrogen in an sp^2-carbon network, preferentially form five-membered rings as some theoretical calculations had shown.
- Was nitrogen capable of doping an amorphous carbon network n-type ?

The next logical step of the study was to simulate the formation of $a-$C:N and then calculate structure and electronic properties. In this chapter density functional *ab initio* molecular dynamics are used to study the incorporation of nitrogen into carbon networks. For this the CPMD (Car-Parrinello Molecular Dynamics) program developed and maintained by the Max Planck Institut fur Festkoperforschung, Stuttgart Germany was used [1]. This program has been used previously to model carbon networks at various densities [2, 3]. CPMD, which uses a quantum mechanical description of electron wavefunctions, is quite different from classical molecular dynamics methods like the Tersoff [4], which have difficulty in describing carbon with sp, sp^2 and sp^3 hybridisations with only a two-centre potential.

The method of simulation was the "liquid quench" technique where a cubic array of atoms is permitted to spontaneously melt. The resulting liquid is allowed to evolve then quenched to 300K and annealed. In recent work, Marks *et al.* [5] have shown that an amorphous structure prepared in a molecular dynamics simulation by the "liquid quench" method is essentially the same as one grown by atom-by-atom condensation. Therefore the "liquid quench" technique can be used to simulate the formation of films deposited using physical vapour deposition techniques.

In the analysis of the simulated networks the Wannier function technique for producing a localized orbital picture within a periodic supercell has been used. This technique has been used by Silvestrelli *et al.* [6] in amorphous silicon, and the theory is explained in detail by Berghold *et al.* [7]. The number of Wannier function centres between atoms identifies the bond type (single, double or triple). In addition, by using Wannier function centres, lone pairs of electrons and different types of nitrogen charged sites can be identified within the networks.

The following section will provide a description of the theoretical foundations of CPMD including: density functional theory; local density approximation; coefficient dynamics; and pseudopotentials. The implementation and reasons for using Wannier functions will also be discussed. This will be followed by a presentation of the results of static substitutional simulations and then the "liquid quench" simulations.

4.2 Density Functional Theory

Density functional theory (DFT) is, quite simply, the solution to the many-bodied problem of electrons in a solid. Hohnberg and Kohn [8] proposed DFT by proving the following two theories:

> **Theorem 1** The many-bodied problem of electrons in a solid may be precisely reduced to the solution of non-interacting one-electron (of the Schrödinger mathematical form) equations coupled by an effective potential which is itself an exact function of the electronic charge density.

The one-electron Schrödinger-like equations are solved self-consistently because the effective potential is a functional of the electronic charge density, which is a function of the solutions to these equations.

> **Theorem 2** The ground state energy of an interacting non-homogeneous electron gas is a unique functional $E[n(\mathbf{r})]$ of the total electron density $n(\mathbf{r})$. Although the functional $E[n(\mathbf{r})]$ is not known, E acquires a minimum value for the ground-state electron charge density n_o.

With the stipulation that the electronic density is non-zero for all points in space and the integral of the electron density gives the total number of electrons N in the system :

$$\int n(\mathbf{r})d\mathbf{r} = N \tag{4.1}$$

Hohnberg and Kohn[8] showed the functional $E[n(\mathbf{r})]$ was in the form:

$$E[n] = \int v(\mathbf{r})n(\mathbf{r})d\mathbf{r} + F[n] \tag{4.2}$$

Kohn and Sham [9] proved that the functional $F[n]$ could be expressed as:

$$F[n] = \frac{1}{2}\int\int \frac{n(\mathbf{r})n(\mathbf{r}')}{|\mathbf{r}-\mathbf{r}'|} + T_s[n] + E_{xc} \tag{4.3}$$

Where the first term is an expression for the Coulombic energy, $T_s[n]$ are the kinetic energy of a system of non-interacting electrons of density n, and E_{xc} exchange-correlation energy of the electron. The exchange-correlation energy describes all other (ie. interactions other than kinetic energy and Coulomb repulsion) electronic interactions.

The expression in eqn(4.3) leads to the Kohn-Sham equations:

$$\left(-\frac{\hbar^2}{2m}\nabla^2 + \int \frac{n(\mathbf{r})}{|\mathbf{r}-\mathbf{r}'|}d\mathbf{r}' + \mu_{xc}[n(\mathbf{r})]\right)\psi_i = \varepsilon_i\psi_i \tag{4.4}$$

$$n(\mathbf{r}) = \sum_i^N \psi_i^*\psi_i \tag{4.5}$$

The ground state energy Φ is found by minimising the functional $E[n(\mathbf{r})]$ with respect to the electronic degrees of freedom ψ_i.

4.2.1 Local Density Approximation

In this work the local density approximation (LDA) to density functional theory is used. This approximates the exchange-correlation energy to be dependent on the electronic charge density at position $\mathbf{r}$:

$$\mu_{xc}[n(\mathbf{r})] \approx \mu_{xc}^{LDA}(n(\mathbf{r})) \tag{4.6}$$

The electronic density in an amorphous solid is a rapidly varying function of position, so the μ_{xc}^{LDA} is approximated to be the same as a uniform volume of some average electronic

density. In each of the simulations presented in this work, a Becke[10] Lee-Yang-Parr[11] generalised gradient approximation (GGA) exchange-exchange correlation functional was used. The GGA approximation extends the LDA to include a term for the gradient of the electron density, not just the average value.

Unpaired singly occupied orbitals cannot be observed using the LDA as it requires each electron orbital to be doubly occupied. In this study the local spin density (LSD) approximation was also used for some calculations. The LSD approximation uses a a separate exchange-correlation functional for spin($\uparrow$) and spin($\downarrow$), and allows the study of unpaired singly occupied orbitals.

4.2.2 Pseudopotentials

Rather than minimise $E[n(\mathbf{r})]$ for all electrons, a pseudo-potential is used to represent the contributions of the core electrons. The pseudo-potentials used in the simulations of amorphous carbon nitride were of the Troullier-Martins [12] norm-conserving type. The pseudopotential was chosen as it converges well for a range of different bonding configurations for carbon and nitrogen.

4.2.2.1 Testing of pseudopotentials

Before simulation of the carbon nitrides, two pseudopotentials were tested to determine their efficacy for simulation of carbon-nitride systems. The two pseudopotentials used were a Martins-Troullier [12]and a Goedecker [13]. The molecules studied were: Cyanogen $(CN)_2$, Pyrrole (C_4H_5N), Imidazole ($C_3H_4N_2$) and Pyrazine ($C_4N_2H_4$). Cyanogen is a linear molecule; Pyrrole is a five-membered aromatic ring containing one nitrogen; Imidazole is a five-membered aromatic ring with two nitrogen atoms - only one of which is bonded to a hydrogen; Pyrazine a six-membered aromatic organic molecule.

For testing all of the molecules were placed in an "isolated" cubic box (isolated refers to using no periodic boundary conditions) and their geometry optimised using CPMD. The size of the box was 12 Å, quite substantial compared to both the molecule size (3-4 Å) and the carbon-nitride simulations ($\approx$ 8Å). For each of the molecules tested there was excellent agreement with expected values and consequently a Troullier-Martins

pseudopotential was chosen as it has been used extensively in other carbon systems with much success.

4.3 Coefficient Dynamics

In their landmark paper of 1985, Car and Parrinello [14] proposed the innovative molecular dynamics scheme within the framework of density functional theory. The basis of the CPMD method is in the *coefficient dynamics* used to allow the electron wavefunctions to follow the motion of the ions. In the technique, the coefficients of the plane-wave basis set vary with time, and are solved in *parallel* to the ionic motion:

$$\mu\ddot{\psi}_i = -\frac{\partial E}{\partial \delta\psi_i^*(\mathbf{r},t)} - \sum_{j=1,N} \Lambda_{ij}\psi_j(\mathbf{r},t) \quad (4.7)$$

$$\mathbf{M}_I\ddot{R}_I = -\nabla_{R_I}E \quad (4.8)$$

$$\mu_\nu = -\left(\frac{\partial E}{\partial \alpha_\nu}\right) \quad (4.9)$$

These equations describe the fictitious classical time evolution of the electronic orbitals ψ_i where μ is the fictitious electronic mass and Λ_{ij} are the Lagrange multipliers required to satisfy the orthonormality constraint on the wavefunctions.

For arbitrary starting values of the fictitious electronic mass μ and of initial conditions $\{\psi_i\}_0\{\dot{\psi}_i\}_0$, thermal equilibration between the classical degrees of freedom $\{R_I\}$ and $\{\psi_i\}$ is achieved after some time through equipartition[15]. If the fictitious electronic mass μ and $\{\psi_i\}_0\{\dot{\psi}_i\}_0$ are chosen so that there is only weak coupling between the two degrees of freedom, transfer of energy between them is small enough to allow adiabatic following of the ionic motion. The occupancy of wavefunctions remains close to their instantaneous Born-Oppenheimer (ground state) surface.

4.3.1 Nóse-Hoover Thermostats

Thermostats are usually used in atomic simulations to guarantee the long-time average of the instantaneous kinetic energy gives the thermodynamic temperature T_0. The Nóse-Hoover equations of motion for N particles and the dimensionless heat-flow variable ζ are:

$$m_i\mathbf{u}_i = F_i - \nu\zeta m_i\mathbf{u}_i \quad (4.10)$$

$$\dot{\zeta} = \nu\left(\frac{T}{T_0} - 1\right) \tag{4.11}$$

where ν is the rate of coupling between the particles and the heat bath at temperature T_0. As expected, if the parameter ν is zero, the motion is Newtonian.

In the CPMD method, the equations of motion for the ions are solved in parallel with the fictitious motion of the electrons. Both the kinetic energy of the ions and fictitious kinetic energy (controlling the coefficient dynamics) can be regulated using a thermostat to prevent the electrons from wandering away from the BO surface. Therefore a separate thermostat is applied to the ions and the electrons.

The ion and electron thermostats were applied during the equilibration at 5000 K with characteristic frequencies ν of 1250 cm^{-1} (as shown in fig (4.1) and 45000 cm^{-1} respectively. During the quenching of the structures from 5000 K the ion temperature was rescaled following a newtonian cooling curve. The energy of the electron thermostat is prescribed [16] by:

$$E_{kin,0} = 10^{-5} \times T \tag{4.12}$$

Where T is in Kelvin, and $E_{kin,0}$ is measured in Hartrees (1 Hartree = 27.2eV).

4.4 Computational Details

In this study the effect of density and nitrogen concentration was studied using different simulations of 64 atom networks using the "liquid-quench" methodology. Six simulations were at densities of 2.45, 2.95 and 3.2 g/cm^3 with two nitrogen concentrations (corresponding to two and eight nitrogen atoms in 64 total) as summarised in Table 4.1. The seventh simulation of 64 atoms were of 2.7 g/cm^3 density and contained four nitrogen atoms. The choice of parameters in the 2.7 g/cm^3 was made for comparison with an experimental carbon nitride study of Walters *et al.* [17]. The eighth simulation was a 64 atom simulation at 2.00 g/cm^3, containing 20 nitrogen atoms to explore nitrogen saturation in low density $a-$C:N.

The "liquid-quench" methodology, as mentioned previously, is as follows: a randomised cubic lattice of atoms is allowed to melt using CPMD, forming a liquid with a tem-

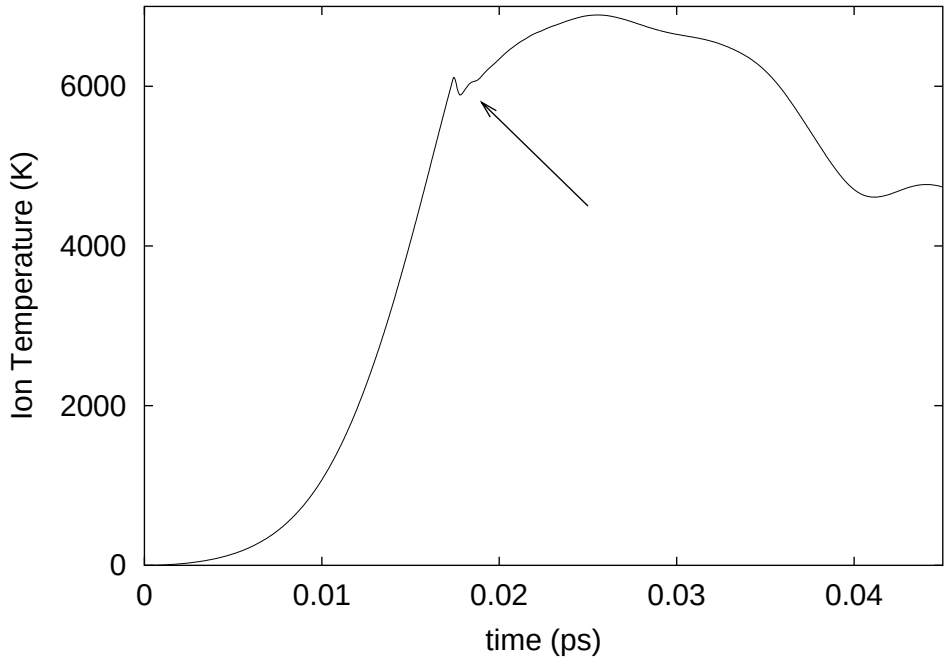

Figure 4.1: Temperature of ions as a function of time during the spontaneous melting of the simple cubic lattice. Nóse thermostats were applied approximately at the point indicated by the arrow.

perature above 4000K which is allowed to equilibrate. The liquid is annealed at this elevated temperature for 0·5 ps. The liquid was then quenched to 300K following a Newtonian cooling equation of the form $T = T_0 e^{-(ct)}$. The quenching time of 0·5 ps is comparable to the quench time expected for a thermal spike following the impact during deposition from an ion beam of energy 50eV [18]. All structures were annealed at 300K for an additional 0·5 ps to enable averaged structure statistics to be collected.

Periodic boundary conditions and Gamma(Γ)-point sampling of the Brillouin zone (BZ) were used. Γ point sampling of the BZ is sufficient for disordered systems because as explained by Remler and Madden [19], disordered systems have a smaller coherence length than a periodic system. Variations between Γ-point calculations and other BZ points are expected to be be minor.

The networks shown in Table 4.1 were formed using the local density approximation (LDA) to density functional theory (DFT). In the LDA, all orbitals are assumed to be doubly occupied, so no unpaired spin orbitals can be studied. This is a reasonable

approximation to employ since it has been found that there is a low number of unpaired spins in amorphous carbon nitride [21]. Also previous *ab initio* simulations of amorphous carbon [2, 3] have shown that the LDA is sufficient to describe bonding in $a-$C. Additional calculations were also performed using the local spin density (LSD) approximation to DFT which does not assume each orbital is doubly occupied. LSD was used in order to check whether the LDA was inhibiting certain bonding configurations. The LSD approximation was also employed to study the effect of charge removal on the network structures.

The energies of the unoccupied states (Kohn-Sham orbitals) were calculated in order to derive the electronic density of states (EDOS) for the simulated structures. The electron localization function was calculated following the method of Becke and Edgecombe [10]. The coordination of each atom was calculated by assuming bonds form within a coordination sphere of 1.85Å. The Debye formula [22] for neutron diffraction was used to calculate the diffracted intensity S(Q),

$$S(Q) = \sum_i \sum_j \frac{f_i f_j sin(Q \cdot r)}{Q \cdot r} \tag{4.13}$$

where $Q = 4\pi sin(\theta)/\lambda$, and r is the distance between atoms and the sum is over all atoms. The radial distribution function g(r) was calculated in real-space and transformed to the reduced density function (pair correlation function) G(r) using the relation $G(r) = 4\pi r\rho(g(r) - 1)$, where r is the radius and ρ the number density (atoms Å^{-3}). The distribution of ring sizes for each network was calculated using the shortest path criteria described by Franzblau [23].

The results and discussion section is divided into three parts, the first covers substituting a nitrogen atom into a pre-defined models of $ta-$C and relaxing the structure. The second section covers models produced using the liquid quench method, while the third section describes charge removal from the end product of the liquid quench models.

4.5 Bonding in simulations of amorphous materials

In a crystalline system, coordination is closely related to bonding, for example carbon in diamond has four nearest neighbours and shares covalent bonds with each of its

neighbours. When symmetry in the system is broken, the relationship between coordination and bonding becomes clouded. An analysis of an amorphous solid is therefore difficult because an analysis of coordination can often be misleading or insensitive to electronic charge distribution.

In a simple measurement of coordination, one can assume that in a simulation, atom A is bonded to atom B if and only if that bond length falls within the first-nearest neighbour (1NN) peak of a $g(r)$ function. A difficulty arises in an amorphous material, for the 1NN of the $g(r)$ has a finite width and does not necessarily fall sharply to zero before or beyond the 1NN peak. One can envisage the 'stretched' or 'compressed' bonds responsible for stress in the amorphous material, as indicated by the 1NN $g(r)$ width.

Another approach which attempts to take into account the presence of bonds is to determine the electron density between two atoms A and B. Areas of high electron density between atoms A and B would indicate a likely bond. A visualisation of electron density in a simulation is shown in fig (4.2), and shows a sequence of images of different electron density. The highest electron density lies around nitrogen atoms, and as seen in fig (4.2)(c), 'dog-bone' shapes of π orbitals can be seen between carbon atoms.

Another example of the electron density is shown in fig (4.3)(a) where in the centre of the figure is a nitrogen atom. The shape shown is an isosurface joining points of like electron density. The sequence (a) to (b) was formed by two geometry optimisations of the same structure under slightly different conditions. In fig (4.3)(b) the nitrogen atom had shifted slightly and the electron density was enhanced between it and a nearby carbon atom. Was this a 'new' bond forming or merely a stretched bond which had shortened ? Another question which is important in carbon nitrides is whether the nitrogen atom is planar or pyramidal as discussed in Section 1.2.2 on page 11 referring to the formation of either a p_z or sp^3 lone pair.

One way to answer the question of whether a given pair of atoms are bonded or not is to evaluate an Electron Localisation Function (ELF). The ELF is a function derived from the idea of Lennard-Jones [24] to measure the probability of finding one electron at (x, y, z) and another of the same spin at (x', y', z'). Lennard-Jones was able to show

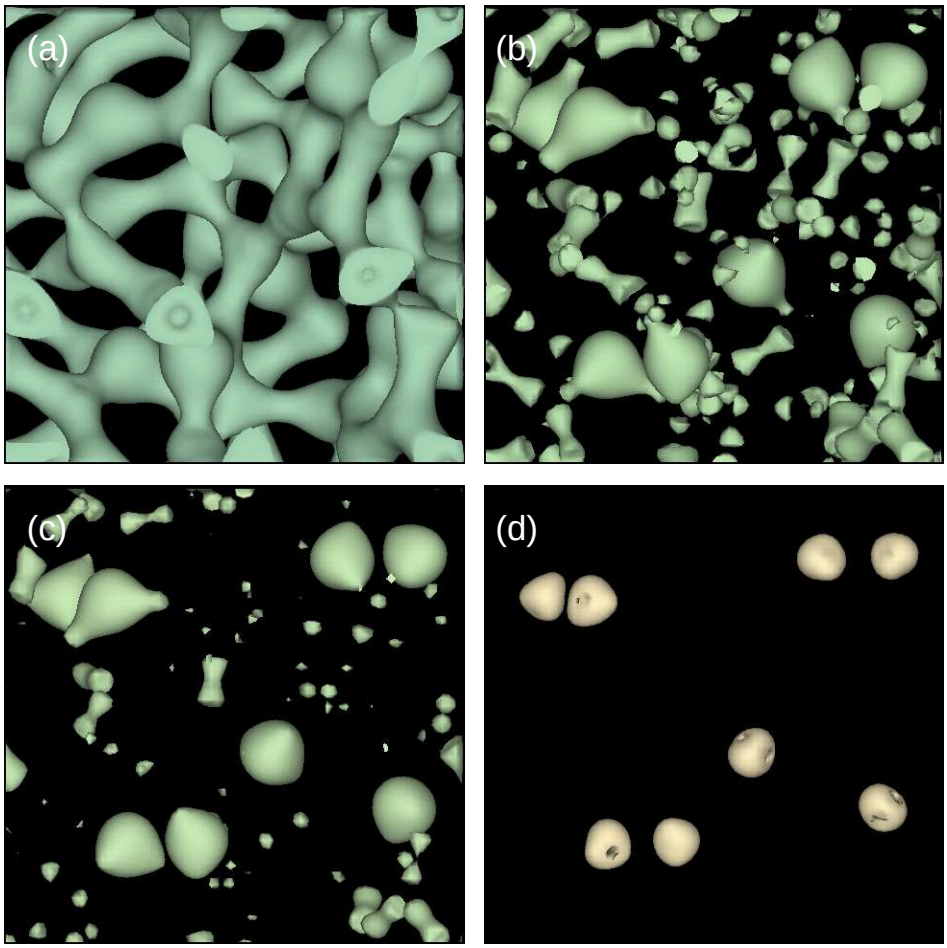

Figure 4.2: Electron density isosurfaces of increasing electron density (a) to (d). regions of highest electron density are centred on each of the eight nitrogen atoms. The "dog-bone" shaped features in (c) are π-bonds between pairs of sp^2-bonded carbon atoms.

that electrons of the same spin occupy different regions, and as there are spin-up and spin-down electrons, these regions (up and down) could overlap. The work of Becke and Edgecombe [10] extended this idea and showed for regions where the probability of like spins was high, so was the delocalization of the electrons high. Conversely, in regions where there was overlap of un-like spins, localisation was higher. An ELF value is between 0 and 1, where 0.5 is for a homogenous electron gas (perfectly delocalised), and 1 is perfectly localised.

ELF functions are evaluated within the CPMD [1] code, and can be visualised as in fig (4.4) which shows the calculated ELF for a three-fold coordinated nitrogen atom

surrounded by three carbon atoms. The parts (a) and (b) of fig (4.4) correspond to two transverse views through the ELF around a nitrogen atom.

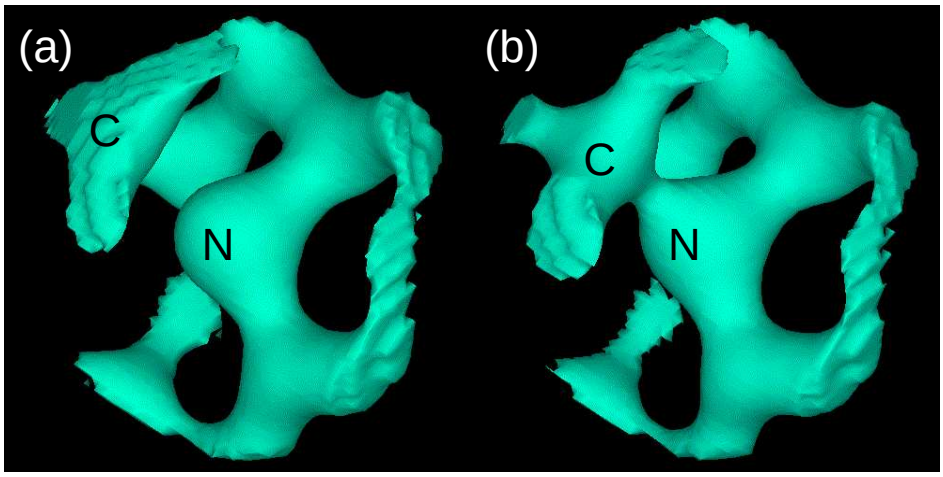

Figure 4.3: Image showing an electron density isosurface (a) before and (b) after an electron charge is removed. Central to the image is a nitrogen atom which appears two-fold using a coordination sphere approach, but may be bonded to the carbon atom top-left in the image. Each image is of the same electron density isosurface. Texture around the edges of the image is an artefact of the finite sampling of the electron density.

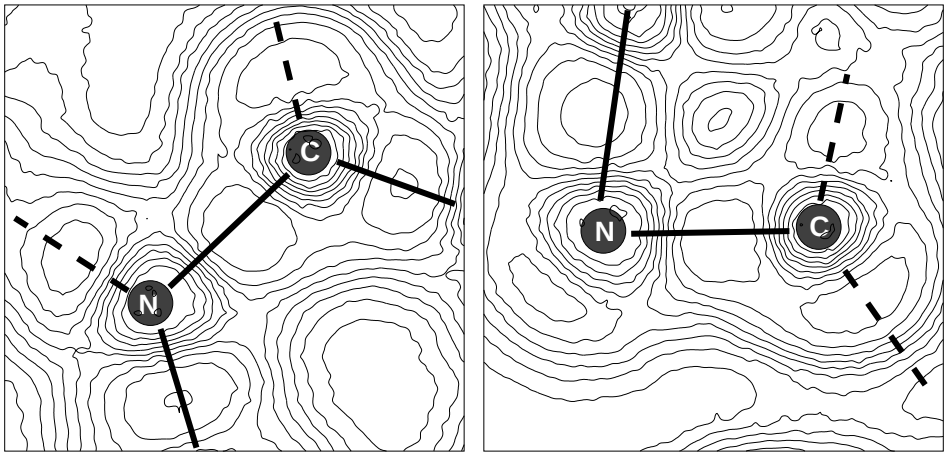

Figure 4.4: ELF function showing a three-fold N bonded to three four-fold C atoms in an amorphous carbon nitride simulation. The two images are in-plane (left) and transverse (right) slices. ELF function is highest where the probability of finding paired electrons is high.

While the calculation of electron density and ELFs proved useful, it was still often inconclusive in an amorphous system like carbon nitride. This was because especially

in situations like fig (4.3), while there was a minute shift in ELF and/or density it was still not a conclusive measure of bonding, or electronic states. This difficulty led to the use of maximally localised Wannier functions, which will be described in the next section.

4.5.1 Wannier Functions

In the analysis of our simulated networks we have used the maximally localised Wannier function technique for producing a localized orbital picture within a periodic supercell. This technique has been used by Silvestrelli *et al.* [6] in amorphous silicon, and again by Fornai *et al.* [25] to examine "floating" bonds in $a-$Si. The number of Wannier functions centres between atoms identifies the bond type (double, single or triple). In addition Wannier functions enable us to identify lone pairs of electrons and types of carbon and nitrogen charged sites within our networks.

A method of generating maximally-localised Wannier functions from the occupied Bloch states has been developed and implemented in the CPMD code [1]. In the Wannier function analysis a unitary transform is applied to express the Bloch states as a sum of orthogonal, localised functions. However, even for the case of a single k-point calculation (used in this study), the unitary transform is not uniquely defined since each Kohn-Sham orbital can be multiplied by an arbitrary phase factor. Marzari and Vanderbilt [26] resolved this by requiring the total spread of Wannier functions to be minimised in real space. To simplify the analysis, rather than visualise the spatial structure of maximally localised Wannier functions, only the Wannier Function Centres (WFC) are calculated. The location of the Wannier-functions x-coordinate x_n (and similarly y_n and z_n) of the nth WFC is given by:

$$x_n = -\frac{L}{2\pi} \quad \text{Im} \quad ln \left\langle w_n | e^{-i\frac{2\pi}{L}x} | w_n \right\rangle \tag{4.14}$$

where L is the length of the supercell and w_n is the n^{th} maximally localised Wannier function. The full details of the calculation can be found elsewhere [6, 7]. The spread in real space of a single wannier function can also be calculated and provides a measure of localisation in real space. Defect states are expected to be less localised than bonding states.

4.6 Simulations of Substituting N into *ta*-C

Using a structure generated using 64 carbon atoms at a density of 2.9 g/cm^3 as the starting point, a single nitrogen atom was substituted at one of the carbon sites and the structure was annealed at 300K. Sites were chosen to test the effect of substituting at both an sp^2 and sp^3 sites. The simulations were performed using a plane wave cut off energy of 35 Rydbergs.

Fig (4.5) shows the effect of substituting a nitrogen atom for a sp^2 bonded carbon atom and equilibrating the structure a 300 K for 13 fs. Very little structural relaxation occurred after the substitution, showing the nitrogen is stable in this configuration. The extra electron due to the presence of nitrogen formed a lone pair with an electron originally in the p_z orbital.

Fig (4.6) shows the corresponding structure following the substitution of nitrogen on an sp^3 site. In contrast to the previous case, this configuration is unstable with an immediate increase in one of the C-N distances, thereby reducing the coordination of the site to 3. This final configuration is similar to that in fig (4.5).

This result ties in well with observation of the limited tolerance of the tetrahedral amorphous carbon structure to nitrogen [27] as discussed in Chapter 1. Experimentally, at concentrations greater than 1%, the network spontaneously transforms from its predominately sp^3 form to a more sp^2 bonded structure.

A similar technique to this was used by Stumm *et al.* [28] who used CPMD to study nitrogen charged sites in diamond-like amorphous carbon by Stumm *et al.* [28], although this was a larger model (216 atoms) the "liquid quench" method was not applied, nor was more than one density considered. Our results were in disagreement to those of Stumm *et al.* who found that a substituting nitrogen into an sp^3-carbon site remained four-fold coordinated. Stumm *et al.* noted this four-fold nitrogen site was only meta-stable configuration and a small displacement of the N atom before relaxation resulted in the N becoming three-fold coordinated. The results of Stumm *et al.* may have reflected the nature of the model used which was a rescaled (from 4.00 g/cm^3 to 3.00

g/cm^3) amorphous diamond structure.

The liquid quench technique gives a more faithful representation of the experimental synthesis of a-C:N films using physical vapour deposition than does the relaxation or substitution methods of Stumm *et al.* [28], because it allows a more complete exploration of the local environment surrounding the N atom.

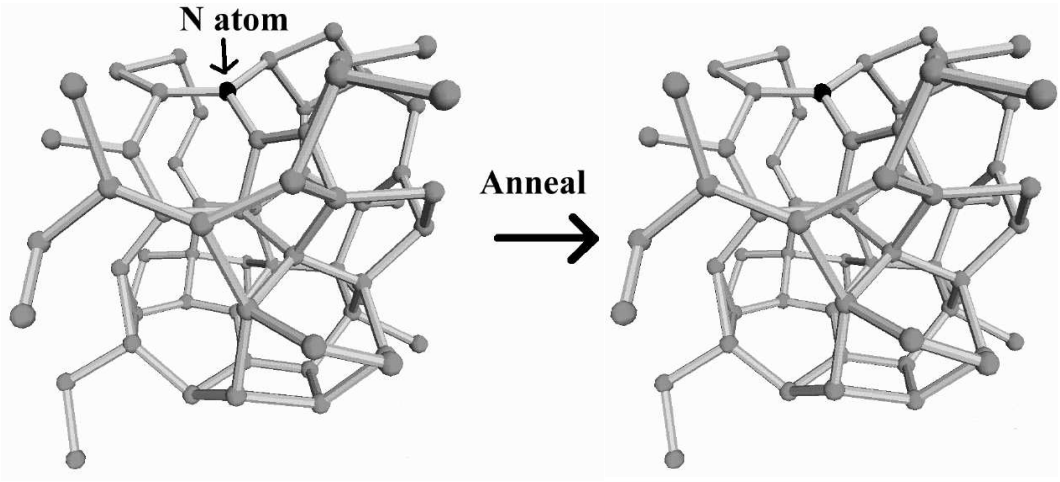

Figure 4.5: The effect of substituting a nitrogen into an sp^2 bonded site (black atom) in a 64 atom tetrahedral amorphous carbon network and annealing at 300 K for 13 fs.

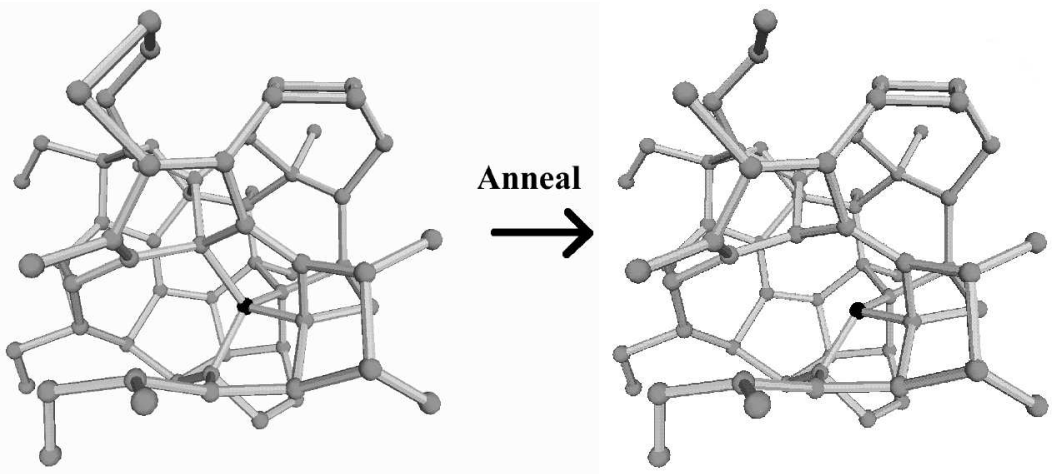

Figure 4.6: The effect of substituting a nitrogen into an sp^3 bonded site (black atom) in a 64 atom tetrahedral amorphous carbon network and annealing at 300 K for 13 fs.

4.7 Studies using Liquid Quench Method

The Wannier function centre analysis gives considerable amount of new information about the bonding in the networks. Carbon and nitrogen atoms in these amorphous networks form single, double or triple bonds with typical bonding arrangements shown in figs 4.7 & 4.8. Also shown is the location of WFCs using small black spheres. For a single (or σ) bond, one WFC is formed between two ions. Between two carbon ions, the WFC is found at the mid-point of the two ions. This can be seen in fig 4.7(a) for an sp^3 bonded C atom with 4 σ bonds. In a carbon nitrogen bond, however, the WFC lies closer to the nitrogen ion giving an indication of the ionicity of the bond see fig 4.8(a). A double bond (or $\sigma + \pi$) forms two WFCs, at 0.7Å from each-other midway between the two ions. An example of this is fig 4.7(b). A triple bond ($\sigma + 2\pi$) forms three WFCs in a triangle between two ions, like in fig 4.8(d) where there is a triple bond between an *sp* bonded C and an *sp* bonded N. The distance between each of the three WFCs is 0.5Å, so the WFCs lie closer together in a triple bond than a double bond.

Another common location of WFCs corresponds to electron lone-pairs forming on nitrogen ions, see fig 4.8(a). Where a lone-pair has formed, a single WFC is found close (0.3–0.4Å) to a nitrogen ion. All of the valence electrons in the networks form one of these three bond-types (single, double triple bonds) or lone-pairs. Dangling bonds are not permitted within LDA because it requires all orbitals to be doubly occupied. Using these definitions of bonds/lone-pairs within the simulated networks, the structures could be analysed in detail. The number of WFCs around an ion enabled us to determine if the atom was sp, sp^2 or sp^3 hybridised without the need to assume bond cut-off distances or coordination shells. In addition, the presence of charged or doping sites could be identified within the networks.

Nitrogen can form a neutral site in two ways: an sp^3 site with 3σ and a lone pair (see fig (4.8)a.) termed an N_3^0, an sp^2 site with 2σ-, a π-bond and a lone pair (see fig (4.8)c) which will be referred to as a N_2^0 site. After identifying these sites, the networks were analysed to determine how many of each type of site they contained, and these results were listed in Table 4.1.

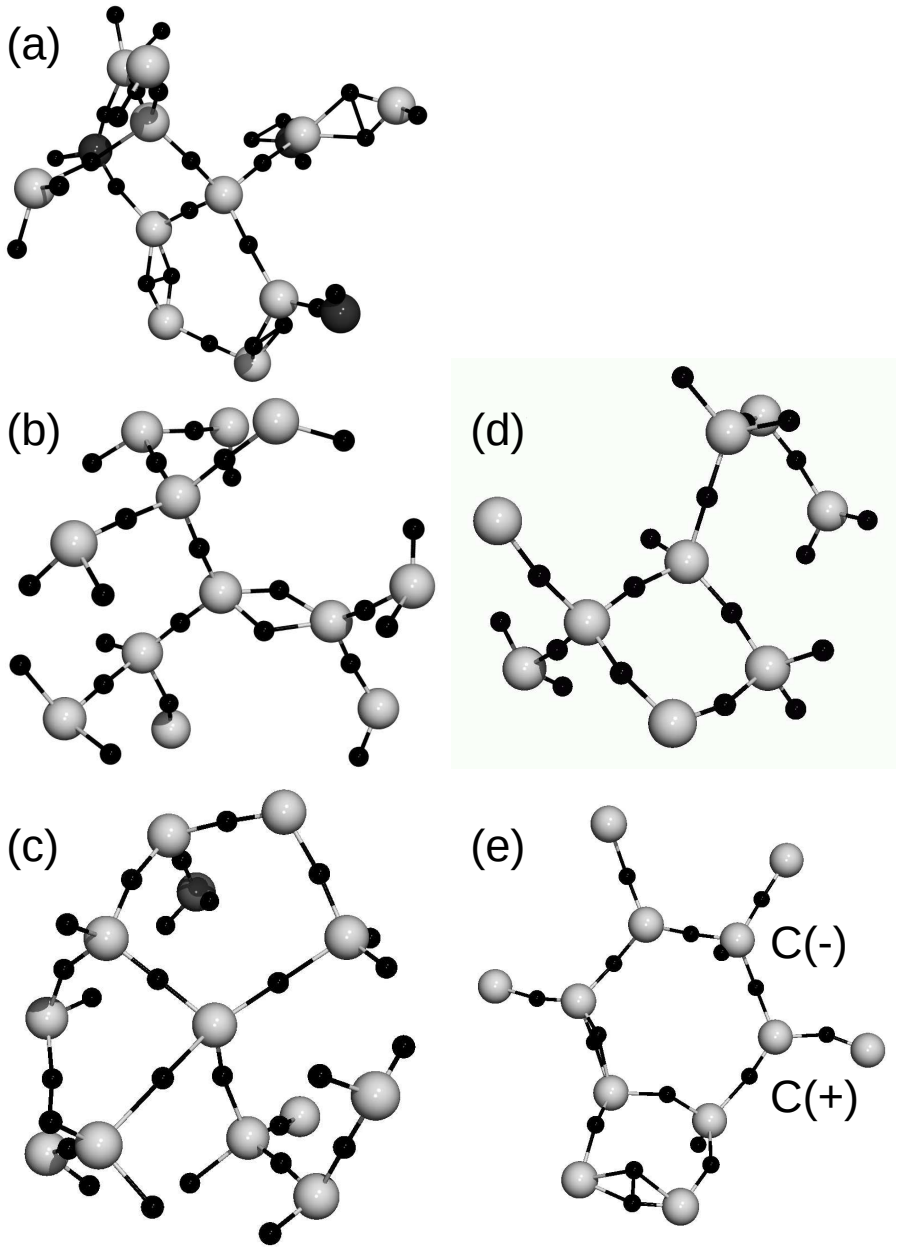

Figure 4.7: Typical arrangements of WFCs (shown as small black spheres) around carbon ions forming single, double and triple bonds. Some locations of WFC also correspond to charged sites. Carbon atoms are shown as light grey, nitrogen atoms as dark grey. The carbon atom labelled C(-) refers to a three-fold carbon atom with an 'extra' WFC not in a bonding location, and is interpreted as having gained an extra electron. The C(+) site refers to a carbon atom surrounded by only three WFC, and has therefore donated an electron to elsewhere in the structure. In doing so the carbon atom now has a relative charge of +1.

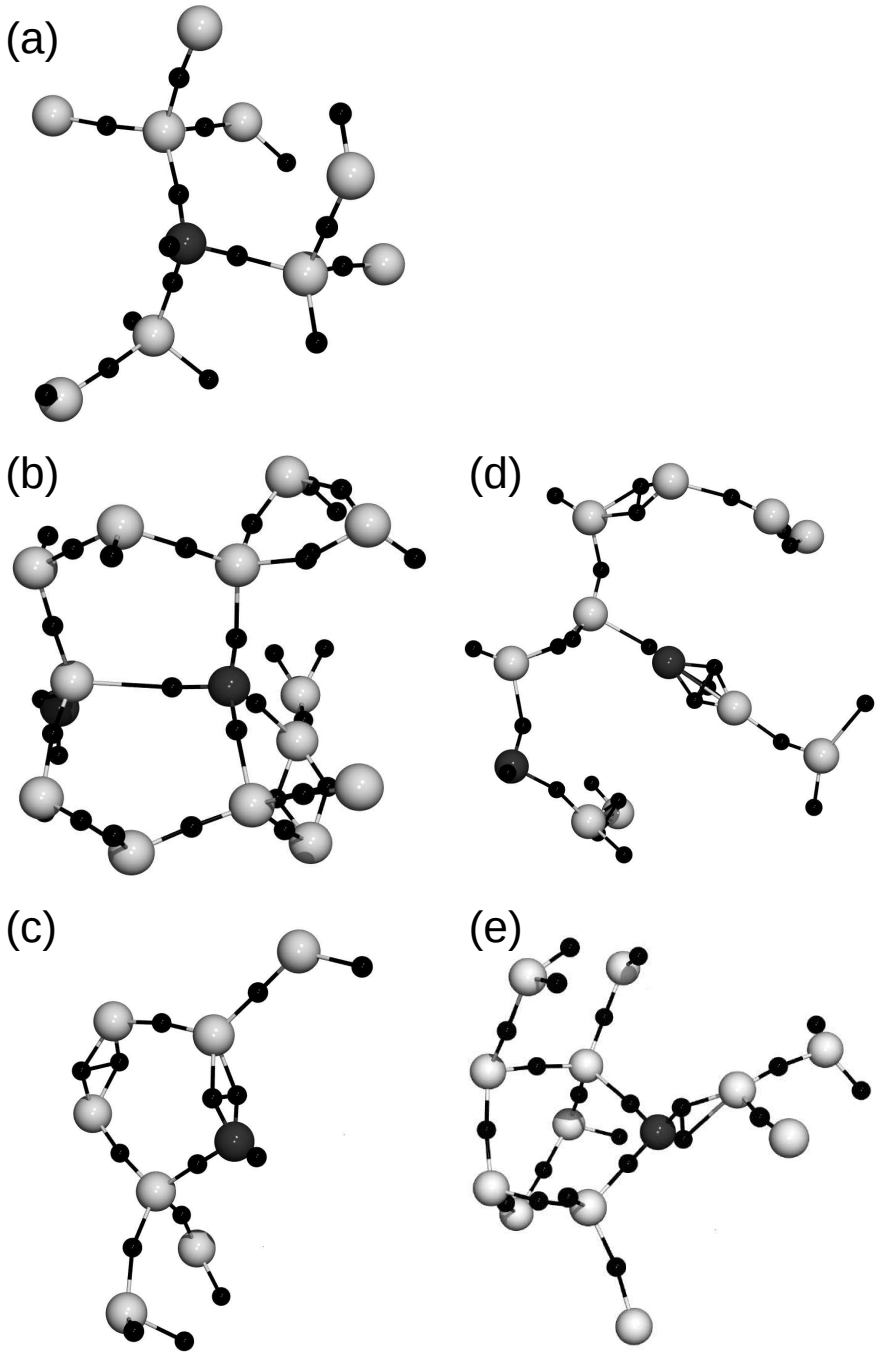

Figure 4.8: Typical arrangements of WFCs (shown as small black spheres) around nitrogen ions forming single, double and triple bonds. Some locations of WFC also correspond to charged sites. Carbon atoms are shown as light grey, nitrogen atoms as dark grey.

Simulation	I C_4^0	II C_3^0	III C_3^+	IV C_3^-	V C_2^0	I N_4^+	II N_3^0	III N_3^+	IV N_2^0	V N_2^+
$C_{62}N_2$-2.45g/cm^3	14	40	3	4	1	-	1	-	-	1
$C_{56}N_8$-2.45g/cm^3	12	40	1	2	1	-	3	1	4	-
$C_{62}N_2$-2.95g/cm^3	38	24	-	-	-	-	2	-	-	-
$C_{56}N_8$-2.95g/cm^3	26	23	2	4	1	1	5	1	1	-
$C_{62}N_2$-3.20g/cm^3	60	2	-	-	-	-	2	-	-	-
$C_{56}N_8$-3.20g/cm^3	41	10	2	3	-	-	6	1	1	-
Total	191	139	8	13	3	1	19	3	6	1

Table 4.1: Bonding details for carbon and nitrogen atoms in all simulations. Higher nitrogen content promotes the formation of charged carbon sites at higher density.

For example in fig 4.8(d) the nitrogen atom forms one single σ bond and one triple bond ($\sigma + 2\pi$) bond to carbon atoms. Since this nitrogen atom originally had five valence electrons and now has only four (one in the σ bond and three in the triple bond) it has donated one electron to the network. With only two neighbours and a positive charge due to the loss of the electron, the nitrogen can be classified as an N_2^+ site.

On the other hand, the carbon atom involved in the triple bond in fig 4.8(d) has four bonding electrons and is therefore uncharged and classified as a C_2^0 site. Using this scheme all the atoms in the networks were classified.

In addition to uncharged sp^3 (C_4^0), sp^2 (C_3^0) and sp (C_2^0) carbon sites, C_3^+ and C_3^- charged sites were observed, see fig 4.7(e). In the case of nitrogen, N_3^0 and N_2^0 uncharged sites as well as N_4^+, N_3^+ and N_2^+ doping sites were observed in the networks. Table 4.1 shows the number of each of these bonding classifications for each of the networks studied.

The most common nitrogen site was the uncharged N_3^0 site, where a nitrogen formed three single σ bonds to carbon atoms and a lone-pair of electrons (see fig 4.8(a) for example), the second most common nitrogen site was the uncharged N_2^0 site with an example shown in fig 4.8(c).

There were three ways nitrogen atoms formed charged sites. The first is shown in fig 4.8(b) which is an sp^3 hybridised nitrogen ion with four bonds. Because this nitrogen has only four valence electrons, it is an sp^3 hybridised N_4^+ site. The second way a nitrogen can bond and form a charged site is when three σ and one π bond form making it an N_3^+ site (see fig 4.8(e)). As discussed earlier, the third way a nitrogen can form a charged site is an *sp* nitrogen forming a triple bond with a carbon (see fig 4.8(d)) - this is termed an N_2^+ site. No circumstances were found where the nitrogen atoms formed a negatively charged site.

4.7.1 Analysis of WFC-Nitrogen-Carbon partial g(r)'s

The ionic structure of the carbon nitrogen networks was analysed by visualising the WFCs as a third species of atom. We monitored the evolution of the WFCs during a 300K anneal, and then calculated the $g(r)$ correlation functions for the network. We found that in the C-N-WFC system the total $g(r)$ is too complicated, and we therefore show only partial $g(r)$ functions $g_{C-WFC}(r)$, $g_{N-WFC}(r)$ and $g_{WFC-WFC}(r)$ from r = 0 to r = 1.5Å. These can be seen in fig 4.9, where the dashed line is the C-WFC $g(r)$, shaded is the N-WFC $g(r)$ and dotted is the WFC-WFC $g(r)$ functions respectively.

From the $g(r)$ analysis we calculated the carbon sp^2 fraction for our networks and compared these to the results of using a coordination shell (r =1·85 Å)as shown in Table (4.2). Table (4.2) reveals that the sp^2 fraction using WFC analysis is fairly consistent with the coordination sphere approach. The largest discrepancy occurred for $C_{62}N_2$-3.2g/cm^3 network, where the carbon sp^2 content was noticeably higher (16%) for the coordination sphere compared to using the WFC (3%). Inspection of the WFCs showed several carbon ions which were thought to be sp^2 were actually bonded sp^3 with an elongated σ-bonds with a bond length greater than 1.85 Å. Other deviations from the coordination were due to either charged charged sites or under-coordination of sites.

In the low density networks $C_{62}N_2$-2.45g/cm^3 and $C_{56}N_8$-2.45g/cm^3, the carbon forms mostly C_3^0 sites with both networks containing a majority (nearly 80%) of 3 coordinate carbon atoms.

	K	Carbon Coordination			Nitrogen Coordination		
Simulation	(GPa)	2	3	4	2	3	4
$C_{62}N_2$-2.45g/cm^3	274	1 (1)	76 (79)	23 (20)	50 (50)	50 (50)	-
$C_{56}N_8$-2.45g/cm^3	273	1 (1)	79 (79)	20 (20)	50 (50)	50 (50)	-
$C_{62}N_2$-2.95g/cm^3	306	0 (0)	39 (44)	61 (56)	50 (0)	50 (100)	-
$C_{56}N_8$-2.95g/cm^3	295	0 (2)	52 (48)	48 (50)	13 (13)	87 (74)	0 (13)
$C_{62}N_2$-3.20g/cm^3	345	0(0)	3 (16)	97 (84)	-	100(100)	-
$C_{56}N_8$-3.20g/cm^3	336	1.6 (1)	23 (20)	76 (79)	12 (12)	75 (75)	-
$C_{60}N_4$-2.70	285.1	2	58	40	25	75	

Table 4.2: Details for the seven amorphous carbon nitride simulations. The percentile value is the coordination of carbon and nitrogen atoms in the simulated networks using a coordination sphere approach (r=1.85Å) and the value in brackets is calculated by analysing the number of WFC surrounding each atom.

The medium density networks $C_{62}N_2$-2.95g/cm^3 and $C_{56}N_8$-2.95g/cm^3 contain mostly C_4^0 sites, with the "increase" of nitrogen (from 2 to 8) leading to a reduction in the number of C_4^0 sites and an increase in C_3^+ and C_3^- charged sites. In the eight nitrogen network N_3^+ and N_4^+ charged sites are also present. The carbon atoms in these networks have a mix of 3 and 4 coordination, with the addition of nitrogen reducing the number of four-fold coordinated atoms.

The medium density networks ($C_{62}N_2$-2.95g/cm^3 and $C_{56}N_8$-2.95g/cm^3) can be compared to the density functional tight-binding (DFTB) simulations of Köhler *et al.*[29] and Weich *et al.* [30] who found similar average carbon and nitrogen coordination at similar N concentrations.

The WFC analysis shows most nitrogen atoms form a lone pair of electrons. Weich *et al.* [30] and Köhler *et al.* [29] also found that nitrogen atoms tend to form lone pairs. However in our simulations we have found significantly fewer numbers of N_3^+ sites (sp^2 hybridised) than Weich *et al.* [30] at a similar density.

Another feature of our simulations was that four-fold coordinated nitrogen sites were rare, with only one case of a N_4^+ in the 2.95 g/cm^3 eight nitrogen structure. This is in

general agreement with Weich *et al.* [30] who found an average nitrogen coordination of 2.85 at 3.00g/cm^3 indicating few if any N_4^+ at a similar density.

A small number of N_4^+ sites is supported by the experimental results of Robertson and Davis [31] who found a low doping efficiency of N in ta-C and attributed it to nitrogen forming non-doping N_3^0 sites.

The high density networks $C_{62}N_2$-3.2g/cm^3 and $C_{56}N_8$-3.2g/cm^3 show the largest differences in bonding two and eight nitrogen simulation. The carbon atoms are mostly 4 coordinated with the addition of more nitrogen dramatically decreasing the number of four coordinate carbon atoms and promoting the number of 3 coordinate carbon atoms.

The highest density (3.2g/cm^3) networks are dominated by sp^3 carbon atoms, as shown in Table 4.2 and 4.3, with 97% in the two nitrogen and 76% in the eight nitrogen cases respectively. As seen experimentally [32] and computationally [29], the increase in nitrogen has increased the carbon sp^2 fraction.

Our results disagree with the theoretical study of Lu *et al.* [33] who studied carbon nitrides by minimising the cohesive energy of 1000 atoms from random positions. They found an increase in nitrogen was accompanied by an increase in the carbon sp^3/sp^2 fraction, whereas we have found an opposite effect. Lu *et al.* also found an increase in nitrogen content was accompanied by a decrease in volume, whereas most experimental studies [27] have seen the opposite effect.

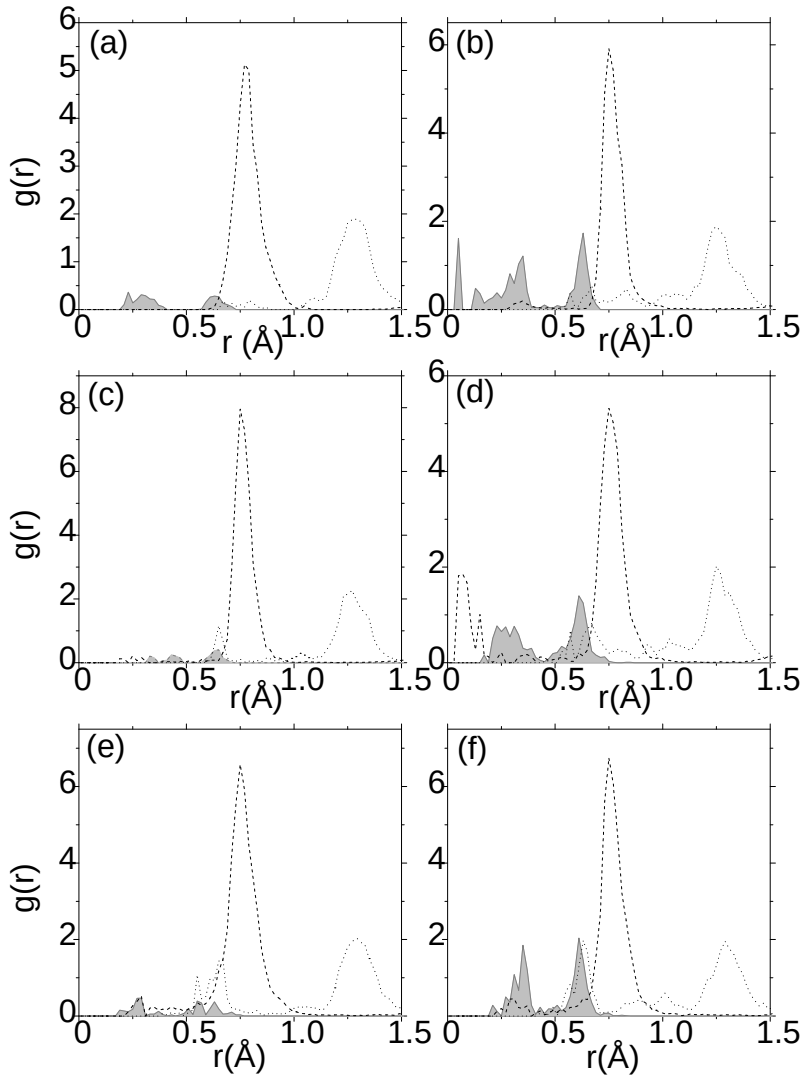

Figure 4.9: The partial correlation functions C-WFC (dash), N-WFC (shaded) and WFC-WFC (dot) for the six simulations - left to right is two (a,c,e) and eight (b,d,f) nitrogen, top to bottom is 3.2 (a,b), 2.95 (c,d) and 2.45 (e,f) g/cm^3. The distribution of distances indicates there are a number of charged states.

The $C_{44}N_{20}$ 2.00 g/cm^3 simulation was performed to evaluate possible mechanisms for nitrogen saturation in low density $a-$C:N. A rendering of the simulated network is shown in fig (4.10). In the image the lighter coloured atoms are nitrogen while the darker are carbon. Two nitrogen dimers can be seen in the image, and two C-N molecules. These molecules were not observed in higher density simulations and in a real deposition may either be lost from the sample or remain trapped in voids and later diffuse out of the structure. The formation of either will limit the nitrogen concentration in a deposited material.

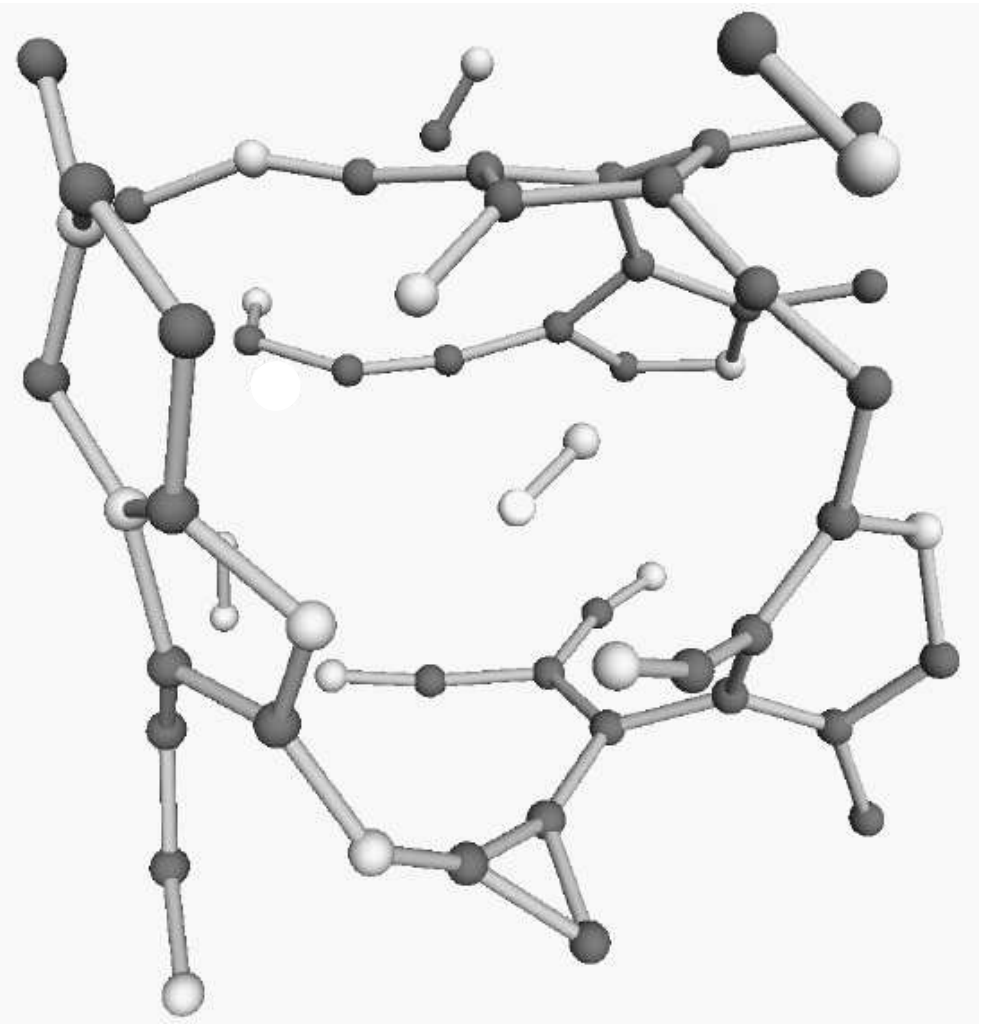

Figure 4.10: An image of the 2.00 g/cm^3 $C_{44}N_{20}$ network showing two nitrogen dimers and two C-N molecules. Light atoms are nitrogen and dark atoms are carbon. Even at this low density a three-membered carbon ring can be observed.

4.7.2 Ring Statistics

The ring statistics of the networks were determined using a coordination sphere approach with a bond-cutoff of 1.85Å. This approach was aided by checking whether the WFC lay between atoms in each ring, or even if some rings had been missed. The low density structures show the majority of rings are five and seven membered.

Each of the networks reveal a different distribution of ring structures, as shown in Table 4.3 and 4.4. Present in all simulations, there are three and four membered rings, and in four instances these four-membered rings contain nitrogen atoms. A general trend is that the addition of nitrogen decreases the number of rings formed due to the formation of lone-pairs, which is most noticeable at the highest density where three-fold coordinated nitrogen atoms prevent the formation of many ring structures compared to 4 coordinated C atoms.

	Number of atoms in ring									
Simulation	3	4	5	6	7	8	9	10	11	12
$C_{62}N_2$-2.45g/cm^3	1	1	10	3	8	3	-	5	2	-
$C_{56}N_8$-2.45g/cm^3	-	2	13	4	3	3	2	-	-	2
$C_{62}N_2$-2.95g/cm^3	4	2	12	23	9	6	1	2	-	-
$C_{56}N_8$-2.95g/cm^3	2	5	8	14	10	11	3	-	-	2
$C_{62}N_2$-3.20g/cm^3	2	2	21	29	26	8	1	-	-	-
$C_{56}N_8$-3.20g/cm^3	2	6	14	14	26	7	1	-	-	-
$C_{60}N_4$-2.70	3	3	8	12	7	4	3	1	-	-

Table 4.3: All Ring Statistics - Bond length cutoff used was 1.85 Å, maximum ring size for the calculation was 12 atoms.

The $C_{56}N_8$-2.45g/cm^3 network shown in fig (4.11) displays clear layering of the structure as suggested by Sjöström *et al.* [34] for a "fullerene-like" amorphous carbon nitride. The layers are spaced at approximately 2.8Å, which is within the range described by Sjöström *et al.* in a gigh-resolution electron micrograph of $a-$C:N. In Table 4.4 it is shown that in this network 7 of the 8 five-membered rings contain nitrogen, suggesting this is an energetically favourable configuration. This agrees with the Hartree-Fock-

	Number of atoms in ring									
Simulation	3	4	5	6	7	8	9	10	11	12
$C_{62}N_2$-2.45g/cm^3	-	-	1	-	1	-	-	1	-	-
$C_{56}N_8$-2.45g/cm^3	-	1	4	3	2(1)	2	1	-	-	(2)
$C_{62}N_2$-2.95g/cm^3	-	1	-	3	2	2	-	-	-	-
$C_{56}N_8$-2.95g/cm^3	-	1	7	6	3	9(1)	3	-	-	-
$C_{62}N_2$-3.20g/cm^3	-	-	2	5	4	3	-	-	-	-
$C_{56}N_8$-3.20g/cm^3	-	1	3	9	15(1)	3(1)	(1)	-	-	-
$C_{60}N_4$-2.70	-	-	1	3	-	1	1	-	-	-

Table 4.4: N atom containing Rings - figure in brackets indicates the number of rings containing two nitrogen atoms in the ring. If the numbers are X(Y) there are X+Y rings containing nitrogen. There were no rings with more than two nitrogen atoms in a ring.

based calculations of Sjöström *et al.* [34] which showed curved sp^2-carbon sheets with five-membered rings containing nitrogen were energetically favourable.

4.7.3 Comparison of angular statistics to other simulations

The medium density networks ($C_{62}N_2$-2.95g/cm^3 and $C_{56}N_8$-2.95g/cm^3) can be compared to the tight-binding simulations of Köhler *et al.*[29] who found similar numbers of two- and three -fold coordinated carbon atoms in a low nitrogen concentration (3%) and about the same proportion of three-fold nitrogen at higher concentrations (11%). Köhler *et al.* also made a measure of the deviation from ideal *sp* and *sp*^{2} geometry of the nitrogen atoms, and this can be inferred from fig (4.12)(c)&(d) which show the bond angle distribution of the two-fold nitrogens is not linear (180°) but quite distorted at around 140°, and the three-fold nitrogens are scattered about an angle of 120°, with some angles are as low as 100°. Using a WFC analysis of the nitrogen atoms shows that most of them form a lone pair of electrons. This disagrees with Köhler *et al.* who classified the three-fold nitrogen bonds as sp$^{(2+x)}$ indicating the nitrogen was not perfectly planar but still *sp*^{2} bonded, whereas it was observed in the simulations that the nitrogen was in a tetrahedral configuration (non-planar) with a lone pair of electrons. Our conclusion is supported by the angular distribution shown in fig (4.11)(c)&(d) which

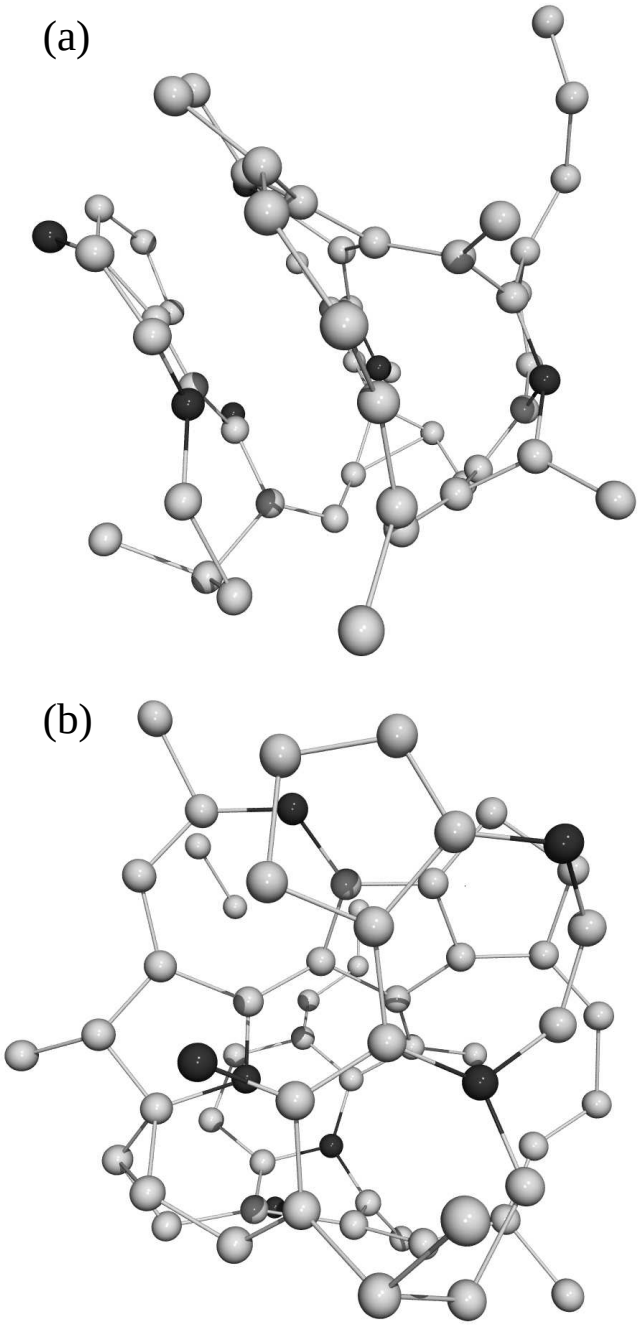

Figure 4.11: Eight nitrogen 2.45g/cm^3 structure revealing fullerene like layering as suggested by Sjöström *et al.* [34]. (a) is a side view, while (b) is perpendicular to the first. Lighter atoms are carbon, darker atoms are nitrogen.

show a majority of the nitrogen bond angles around 109° for these two structures. The carbon angular distribution has a maximum at bond angles between 110 and 120° as observed in amorphous carbon simulations [3].

4.7.4 Comparison to neutron diffraction data

There was no diffraction data available for the stoichiometries of the six simulated networks, so to compare the simulations with experiment, a seventh simulation was performed with 60 carbon and 4 nitrogen atoms with a density of 2.7g/cm^3. The structure contained a majority (58%) of carbon atoms which are three-fold coordinated. The radial distribution function G(r) shown in fig 4.13(a) is compared to the experimental data from Walters *et al.* [17] for a 2.7 g/cm^3 5% nitrogen a-C:N, the agreement is good for both G(r) and S(Q) over which comparison is valid. The region on S(Q) at low Q (<2Å^{-1}) contains a contribution from the size and shape of the cell and should be ignored.

4.7.5 Bulk Modulus

The calculated bulk modulus (K) was calculated by varying the lattice parameter by up to 1% and fitting elastic constants assuming a cubic system. The result for each network is shown in Table 4.2. As expected, there is an increase in K with density. These calculations show that the addition of nitrogen on the order of 3 to 11% does not significantly affect the bulk modulus of the amorphous structures. Our highest values are only 10% lower than those calculated by Lu *et al.* [33] which is surprising considering the mass density used in Lu *et al.* was 6 g/cm^3, considerably higher than any of the networks simulated here.

4.7.6 Electronic Density of States

The electronic density of states (EDOS) determined from the Kohn-Sham Energy calculations are shown in fig 4.14. For the sake of this comparison the Fermi energy is considered to be at the highest occupied state (solid lines). The unoccupied states are plotted with dashed lines.

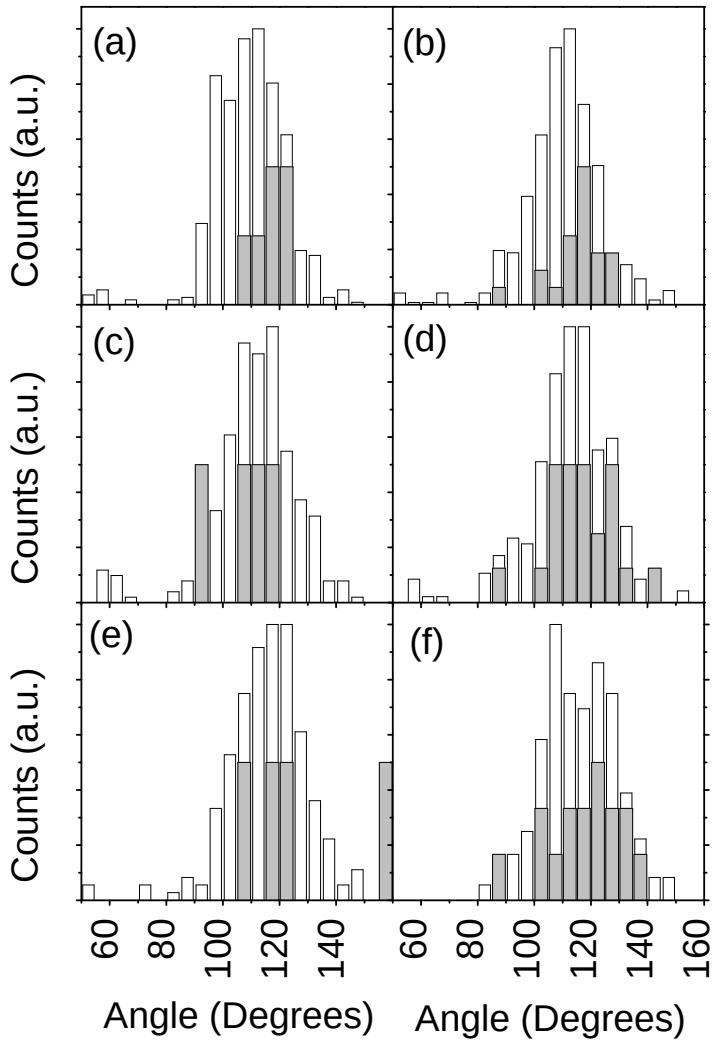

Figure 4.12: The angle statistics for carbon and nitrogen (shaded) for each of the six simulations, (a), (c) and (e) represent the 3.20, 2.95, and 2.45 g/cm^3 $C_{62}N_2$ networks respectively and (b), (d) and (f) the 3.20, 2.95 and 2.45 g/cm^3 $C_{56}N_8$ networks respectively.

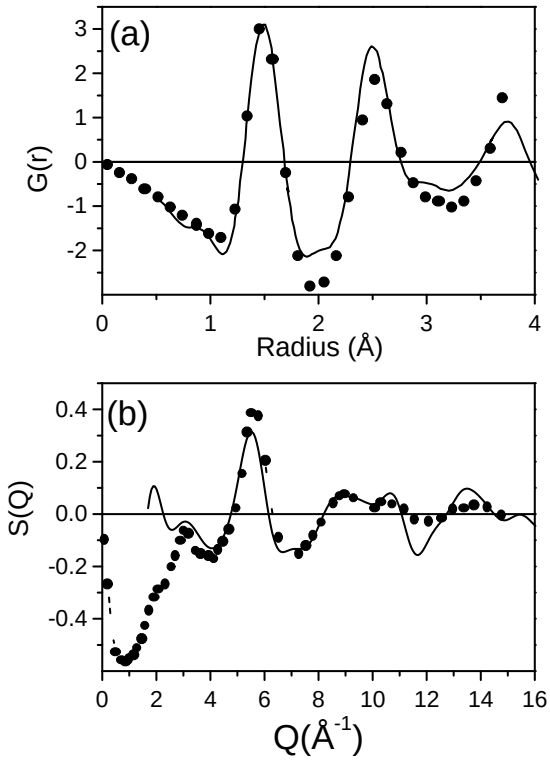

Figure 4.13: The radial distribution function G(r) and S(Q) calculated for 2.7 g/cm^3 $C_{60}N_4$ simulation. In (a) the solid line represents the simulated G(r) smoothed using an sbezier, the symbols represent scaled data from sample CN05 from Walters *et al.* [17]. In (b) the dotted line is the experimental data from the same sample CN05 from Walters *et al.* using neutron diffraction.

In general the higher densities have the fewest states in the "gap" while at lower densities there is no "gap" between the highest occupied molecular orbital (HOMO) and the lowest unoccupied molecular orbital (LUMO).

The two and eight nitrogen 2.45g/cm^3 EDOS fig 4.14(e,f) has a large number of occupied and unoccupied states close to the Fermi energy indicating these structures are potentially good conductors. Of interest is the intensity of the 1s – π^* region of the carbon K-edge, which will be considered 0–5eV above the LUMO. It is this feature which is used to obtain a measure of the π bonding in the material using electron energy loss spectroscopy (EELS) or x-ray absorption spectroscopy (XAS). There is a clear

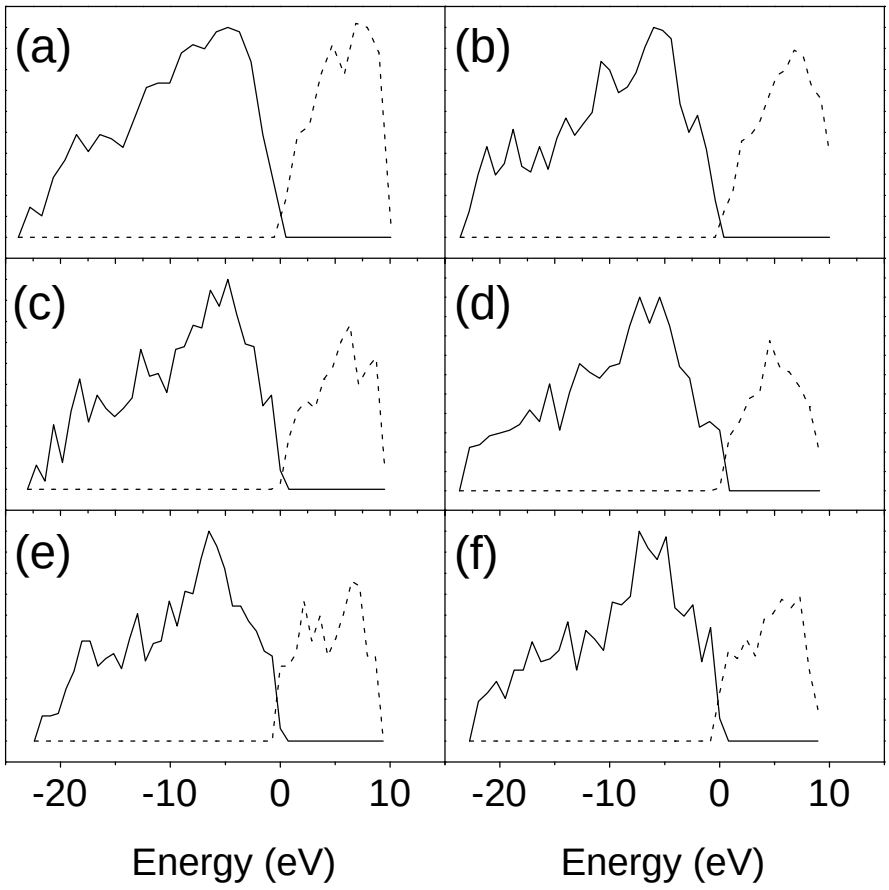

Figure 4.14: The Kohn-Sham energies calculated for six simulations. (a), (b) and (c) represent the 3.20, 2.95 and 2.45 g/cm^3 $C_{62}N_2$ respectively, while (d) (e) and (f) are for the 3.20, 2.95 and 2.45 g/cm^3 $C_{56}N_8$ respectively. The solid line represents occupied states, the dotted line unoccupied states. Each plot is the summation of ten calculations.

shoulder in the 1s – π^* region in both the two and eight nitrogen cases at 2.45 g/cm^3. A large 1s – π^* feature is a consequence of the large number of three-fold coordinated carbon atoms and the number of two-fold coordinated carbon and nitrogen atoms in these structures. Table 4.5 compares the integral of the number of states in this region compared to the fraction of two- and three-fold coordinated bonding in each of the networks. There is an increase in the number of states in this region as the number of nitrogen atoms increases (4.9 to 5.9 in Table 4.5). The enhancement of the 1s - π^* feature as N content increases has been seen experimentally [32].

The intensity in the 1s – π^* diminishes as the density of the networks increase, and the edge of the occupied states becomes steeper . This effect was also seen by Köher *et al.* [29]. The highest density (3.2g/cm^3) structure exhibits the largest "gap". The low number of states between 0-5eV is consistent with the characteristic "diamond-like" C and N-K edges seen in experimental EELS spectra at low nitrogen concentrations [27].

Simulation	Unoccupied States	C sp^2+sp (%)
$C_{62}N_2$-2.45g/cm^3	4.9	80
$C_{56}N_8$-2.45g/cm^3	5.9	80
$C_{62}N_2$-2.95g/cm^3	3.6	44
$C_{56}N_8$-2.95g/cm^3	3.9	50
$C_{62}N_2$-3.20g/cm^3	3.2	16
$C_{56}N_8$-3.20g/cm^3	3.3	30

Table 4.5: Integrated Unoccupied States grouped by number of nitrogen atoms per simulation and density.

4.7.7 Calculations using the LSD approximation

In order to check whether the LDA was inhibiting certain bonding configurations and to explore the effect of removing electrons, calculations were performed on the simulated structures using LSD instead of LDA. A structure from near the end of the 300K anneal for each density was chosen and a geometry optimisation was performed using both LDA and LSD and the structures compared. There were no significant differences

between the LDA and LSD optimised structures.

Further analysis of the LSD relaxed structures was then performed to study the effect of removing one electron. Charge removal corresponds to ionisation and any subsequent structural relaxation would have important consequences in the study of ta-C:N as an electronic material. In order to check the reversibility of any structural relaxation, the electron was replaced and the charge neutral structure was re-optimized. The effect of an electron removal was then determined by comparing the electronic charge densities and bond lengths of each structure at each of the steps.

The 2.45g/cm^3 structures were not measurably affected by the removal of one electron. However in the 2.95g/cm^3 two nitrogen network upon removal of an electron we observed a new bond between a three-fold coordinated carbon atom and two-fold coordinated nitrogen atom. This bond formation after charging is shown in fig 4.14. The formation of a bond is interesting because it showed that charging the system could result in structural change, and it also shows that this structural change may be localised on the nitrogen atoms for an N doped ta-C system.

In the eight nitrogen 3.20 g/cm^3 one nitrogen atom switched bonds from one four-fold carbon to another three-fold carbon as a result of charging. These observations support the concept that the nitrogen atoms are a source of local structural instability in agreement with experimental observations that high density ta-C:N is less stable in an electron beam than undoped ta-C [27]. In addition, restoring the electron was found to only return the structure to its original condition provided that no new bonds had formed in the vicinity. This may explain the observed two-state conductivity which is observed in a-C:N [35]. The local structural changes caused by the removal of an electron prevent the easy recapture of the electron to the nitrogen atom, giving rise to the observed hysteresis or 'memory'.

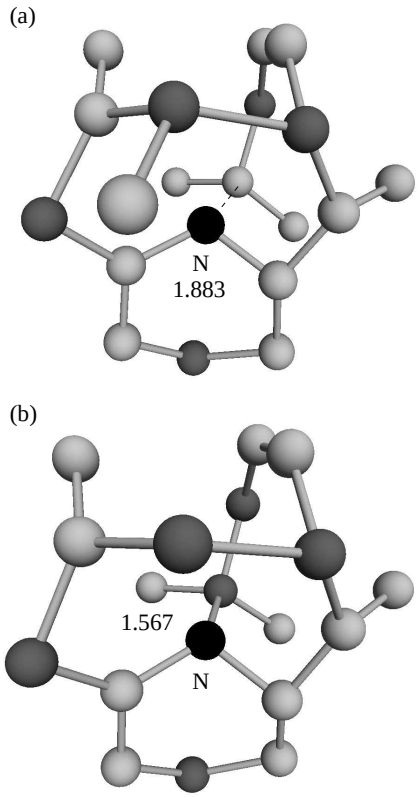

Figure 4.15: Charging experiment for $C_{62}N_2$ 2.95 g/cm^3 showing (a) before an electron is removed from the structure and (b) a bond forming after. The distances shown are in Angstroms.

4.8 Conclusion

Ab initio molecular dynamics has been used to study the structure and bonding of amorphous carbon nitride at a range of densities and nitrogen concentrations. By calculating the centres of maximally localised Wannier functions it is possible to distinguish between the different bonding types present in the networks. The main findings of these simulations are:

- The most common form of nitrogen bonding was found to be uncharged N_3^0 sites with a lone pair of electrons. Uncharged N_2^0 sites as well as charged N_4^+, N_3^+ and N_2^+ were also found.
- At high nitrogen concentration, N_2 dimers and C-N molecules were observed supporting the experimental observation of nitrogen saturation in an $a-$C matrix.
- Addition of nitrogen causes a decrease in the sp^3 fraction of carbon, and this effect is most severe at high densities. In addition to sp^3 and sp^2 bonded carbon, sp (C_2^0), C_3^+ and C_3^- charged sites were also observed.
- Electronic density of states calculations shows an increase in the 1s–π^* region at lower network densities and higher nitrogen concentrations as seen experimentally.
- The removal of electrons from the networks caused structural changes which could explain the two-state conductivity in ta-C:N memory devices.

Bibliography

[1] J. Hütter, A. Alvi, T. D. M. Bernasconi, S. Goedecker, D. Marx, M. Tuckerman, and M. Parrinello, MPI für Festkorperforschung and IBM Zurich Research Laboratory **v3.0–3.3,** 1995–1999 .

[2] N. A. Marks, D. R. McKenzie, B. A. Pailthorpe, M. Bernasconi, and M. Parrinello, Physical Review B **54,** 9703 (1997).

[3] D. G. McCulloch, D. R. McKenzie, and C. M. Goringe, Physical Review B **61,** 2349–2355 (2000).

[4] J. Tersoff, Phys. Rev. B **37,** 6991 (1988).

[5] N. A. Marks, D. G. McCulloch, and D. R. McKenzie, submitted .

[6] P. L. Silvestrelli, N. Marzari, D. Vanderbilt, and M. Parrinello, Solid State Communications **107,** 7–11 (1998).

[7] C. Berghold, C. Mundy, A. Romero, J. Hütter, and M. Parrinello, Physical Review B **61,** 10040–10048 (2000).

[8] P. Hohnberg and W. Kohn, "Inhomogenous electron gas," Physical Review **136,** 865 (1964).

[9] W. Kohn and L. J. Sham, "Self-consistent equations including exchange and correlation effects," Physical Review **140,** 1133 (1965).

[10] A. D. Becke and K. E. Edgecombe, Journal Chemical Physics **92,** 5397–5403 (1990).

[11] C. Lee, W. Yang, and R. G. Parr, Physical Review B **37,** 785 (1988).

[12] N. Troullier and J. L. Martins, "Efficient pseudopotentials for plane-wave calculations," Physical Review B **43,** 1993–2006 (1991).

[13] S. Goedecker, M. Teter, and J. Hutter, "Seperable dual-space Gaussian pseudopotentials," Physical Review B **54,** 1703–1710 (1996).

[14] R. Car and M. Parrinello, "Unified approach for molecular dynamics and density-functional theory," Physical Review Letters **55,** 2471 (1985).

[15] G. Galli, R. M. Martin, R. Car, and M. Parrinello, "*Ab initio* calculation of properties of carbon in the amorphous and liquid states," Physical Review B **42,** 7470–7482 (1990).

[16] P. E. Blöchl and M. Parrinello, "Adiabaticity in first-principles molecular dynamics," Physical Review B **45,** 9413–9416 (1992).

[17] J. K. Walters, M. Kühn, C. Spaeth, H. Fischer, F. Richter, and R. J. Newport, "Neutron-diffraction studies of amorphous CN_x materials," Physical Review B **56,** 14315–14321 (1997).

[18] N. A. Marks, Physical Review B **56,** 2441–2446 (1997).

[19] D. K. Remler and P. A. Madden, "Molecular dynamics without effective potentials via the Car-Parrinello approach," Molecular Physics **70,** 921–966 (1990).

[20] A. D. Becke and K. E. Edgecombe, Physical Review A **38,** 3098 (1988).

[21] F. Demichelis, X. F. Fong, A. T. S. Schreite and, and C. E. Martino, Diamond and Related Materials **4,** 361–365 (1995).

[22] *X-Ray Diffraction*, B. E. Warren, ed., (Addison-Wesley Publishing Company, Reading MA, 1969).

[23] D. S. Franzblau, "Computation of ring statistics for network models of solids," Physical Review B **44,** 4925 (1991).

[24] J. E. Lennard-Jones, Journal of Chemical Physics .

[25] M. Fornari, N. Marzari, M. Peressi, and A. Baldereschi, Computational Materials Science **20,** 337–342 (2001).

[26] N. Marzari and D. Vanderbilt, Physical Review B **56,** 12847–12865 (1997).

[27] C. A. Davis, D. R. McKenzie, Y. Yin, E. Kravtchinskaia, G. A. J. Amaratunga, and V. S. Veerasamy, Philosophical Magazine B **69,** 1133–1140 (1994).

[28] P. Stumm, D. A. Drabold, and P. A. Fedders, Journal of Applied Physics **81,** 1289 (1997).

[29] T. Köhler, G. Jungnickel, and T. Frauenheim, Physical Review B **60,** 10864–10871 (1999).

[30] F. Weich, J. Widany, and T. Frauenheim, Phys. Rev. Lett. **78,** 3326 (1997).

[31] J. Robertson and C. A. Davis, Diamond and Related Materials **4,** 441–444 (1995).

[32] J. Hu, P. Yang, and C. M. Leiber, Physical Review B **57,** R3185 (1998).

[33] Y. F. Lu, Z. F. He, and Z. M. Ren, Journal of Applied Physics **86,** 5417–5421 (1999).

[34] H. Sjöström, S. Stafström, M. Boman, and J.-E. Sundgren, Phys. Rev. Lett. **75,** 1336–1339 (1995).

[35] E. G. Gerstner and D. R. McKenzie, Solid state Electronics **44,** 1641–1645 (2000).